

Resolution and apodization in images generated by twin photons

Ivan F. Santos, M. A. Sagiuro, C. H. Monken, and S. Pádua*

Departamento de Física, Universidade Federal de Minas Gerais, Caixa Postal 702, 30123-970 Belo Horizonte MG, Brazil

(Received 8 September 2002; published 26 March 2003)

We show that an image of an object is obtained when at least one of the photons of a parametric down-converted pair illuminates the object and the two photons are detected in coincidence after they have been transmitted by two lenses. The image is mathematically described by a quantum fourth-order correlation function that differs from the classical image description in two aspects. The quantum image is produced by a nonlocal effective lens whose aperture is described by a compressed convolution of the magnitude of lens transmission functions. The image is generated by the entangled state two-photon light source in which the effective wavelength is equal to the de Broglie wavelength $\lambda/2$, where λ is the wavelength associated to the individual photons. Images can be obtained with a resolution better than the obtained with coherent classical light sources. Better resolution and strong apodization effects are observed.

DOI: 10.1103/PhysRevA.67.033812

PACS number(s): 42.50.Ar

I. INTRODUCTION

The use of optical parametric processes as light sources for the generation of images has been the subject of some recent and promising works. For sources with a large number of photons, optical parametric amplifiers and oscillators, quantum aspects of image formation have been studied: generation of pairs of entangled optical images [1], reduced noise amplification of input images in parametric amplifiers [2,3], and quantum limits imposed by quantum fluctuations in optical images [4]. At the level of single photon pairs, a few works have studied image formation. An entangled two-photon field is generated by spontaneous parametric down conversion (SPDC). In the process of SPDC, a pump (p) laser beam incident upon a nonlinear crystal creates a pair of photons, usually called signal (s) and idler (i) [5]. Imaging of objects illuminated by photon pairs and detected in coincidence was proposed in Ref. [6] and demonstrated experimentally by Pittman *et al.* [7]. More recently, Abouraddy *et al.* have studied the role of entanglement in a two-photon image [8] and have developed a general Fourier-optics theoretical treatment of image formation for the SPDC process [9].

In this work, we studied theoretically the image formation of an object when illuminated by at least one of the photons generated by SPDC. Our main motivation is to investigate the possibility of using entangled photon pairs for generating images with resolution better than the diffraction limit. In 1995, Jacobson *et al.* [10] proposed that a de Broglie wavelength can be associated to a multiphoton wave packet, in the same way it is done for bound massive particles. For a system of N photons, the resultant wavelength is $\lambda_{dB} = \lambda_i/N$, where λ_i is the wavelength associated to the individual constituent photons (the photon wave packet central wavelength). In 1999, Fonseca, Monken, and Pádua [11] demonstrated experimentally the predictions of Jacobson *et al.*, with a double slit setup that can be considered as an analog setup to that proposed in Ref. [10]. Young interference patterns of the two-photon wave packets, which behaved like single entities with twice the energy of each constituent pho-

ton, were detected. The corresponding wavelength was, of course, half the de Broglie wavelength of a single photon. If N photons in an entangled state can behave as a single entity of de Broglie wavelength λ/N , many applications can be envisioned. The two-photon lithography has been proposed recently [12], for beating the diffraction limit. Another application is to generate images of an object by illuminating it with light generated by SPDC. Since the photon pairs generated by this process can be in a momentum entangled state, the de Broglie wavelength of the pair is $\lambda/2$. This suggests that an image obtained with this light source may beat the diffraction limit of the image resolution [13]. If this is true, although the twin photons have wavelength λ (in general in the infrared), the lens aperture diffraction would have maximum separations as produced by a light source with wavelength $\lambda/2$ (commonly in the ultraviolet). By Rayleigh criterion, this would mean that the image resolution would be better than that obtained with coherent classical light sources.

Initially, we suppose that an image of an object is formed at the image plane when the object is illuminated by light in the two-photon state generated by the collinear SPDC [Fig. 1(a)]. Photons transmitted by the object are collected by a lens and split by a 50-50 beam splitter. The image is obtained by detecting the photon pairs at the image plane position in coincidence with two spatially separated detectors. By using a quantum multimode formalism, we have calculated the quantum fourth-order correlation function at the image plane for this optical scheme. A general expression is obtained and we show that, in general, the fourth-order correlation as a function of the detector positions does not generate an image of the object. We propose then three slightly different optical configurations in which the fourth-order correlation function produces the image of the object. A general mathematical expression is obtained for the quantum spatial fourth-order correlation function for the three proposed optical configurations. This expression differs from the classical intensity distribution at the image plane in two aspects. In the quantum fourth-order correlation function the wavelength that appears is the two-photon de Broglie wavelength $\lambda/2$. Secondly, the magnitude of transmission function that describes the lens aperture is an effective one, which is equal to the “reduced”

*Email address: spadua@fisica.ufmg.br

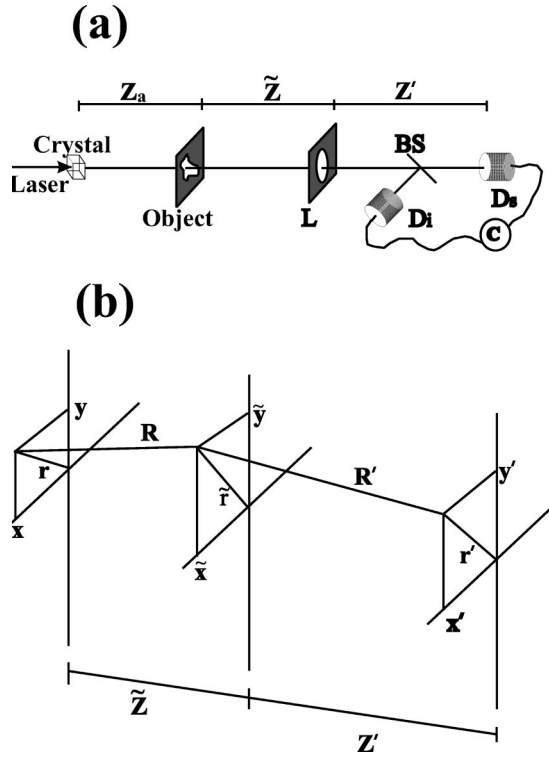


FIG. 1. (a) Outline of the proposed experimental setup for observing the image of an object illuminated by collinear parametric down-converted photon pairs, after a laser beam is incident on a type II crystal. The image is detected in coincidence at the image plane by signal D_s and idler D_i detectors. L is a lens, BS is a polarized beam splitter, z_a is the crystal-object distance, \tilde{z} is the object-lens distance, and z' is the lens-image distance. (b) Coordinates involved in the process of image formation. R is the distance from a point (x, y) in the object to a point (\tilde{x}, \tilde{y}) at the lens and similarly R' is the distance from a point (\tilde{x}, \tilde{y}) in the lens to a point (x', y') at the image plane.

convolution of the magnitudes of the lens apertures “seen” by the idler and signal photons. A quantum nonlocal image of the object is generated. In Sec. II, we review the classical calculation of the electric field distribution at the image plane for a coherent object. The probability amplitude for detecting photons idler and signal at the image plane is calculated in Sec. III. A comparison between the classical and quantum predictions is discussed in Sec. IV and we conclude in Sec. V.

II. CLASSICAL PROCESS OF IMAGE FORMATION

The classical theory of image formation is based on the phase altering characteristics of a lens [13]. We consider here image formation for objects smaller than the transverse coherence length of the light at the object position, called coherent objects. The object is illuminated and the transmitted light is collected by a lens with a focal length f , separated from the object by a distance \tilde{z} . The image detection is done at the image plane that is far from the lens by a distance z' . Those distances are related by the thin-lens formula

$$\frac{1}{f} = \frac{1}{\tilde{z}} + \frac{1}{z'}. \quad (1)$$

Figure 1(b) shows the coordinates at the object plane xy , lens plane $\tilde{x}\tilde{y}$, and image plane $x'y'$. The propagation of the electric field from the object to the image plane is obtained from the Fresnel-Kirchhoff diffraction integral. The electric field at the image plane is written as a function of the electric field immediately before the object $E(x, y)$, the transmission function of the object $A_0(x, y)$, and the transmission function of the lens $A_L(\tilde{x}, \tilde{y})$:

$$E'(x', y') = \text{const} \times \int \int \int \int E(x, y) A_0(x, y) A_L(\tilde{x}, \tilde{y}) \times \frac{e^{ik(R'+R)}}{R'R} dx dy d\tilde{x} d\tilde{y}, \quad (2)$$

where R is the distance from a point (x, y) in the object to a point (\tilde{x}, \tilde{y}) at the lens and similarly R' is the distance from a point (\tilde{x}, \tilde{y}) in the lens to a point (x', y') at the image plane [Fig. 1(b)]. The transmission function of the lens $A_L(\tilde{x}, \tilde{y})$ has the following form:

$$A_L(\tilde{x}, \tilde{y}) = |A_L(\tilde{x}, \tilde{y})| \exp\left[-\frac{ik(\tilde{x}^2 + \tilde{y}^2)}{2f}\right], \quad (3)$$

where $|A_L(\tilde{x}, \tilde{y})|$ describes the size of the lens, being equal to 1 where the lens aperture is transparent and 0 outside it. By considering the object and its image relatively small when compared with \tilde{z} and z' , the factor $1/R'R$ in Eq. (2) can be approximated by a constant. The phase $ik(R'+R)$, after being written as a function of transverse and longitudinal coordinates [see Fig. 1(b)], is simplified by a Taylor first-order expansion [13] and by the use of Eq. (1). A condensed expression can then be derived for the electric field at the image plane

$$\vec{E}'(\vec{r}') = \text{const} \times \int d\vec{r} A_0(\vec{r}) T_L\left(k\left(\frac{\vec{r}}{\tilde{z}} + \frac{\vec{r}'}{z'}\right)\right), \quad (4)$$

where we have defined the transverse coordinates $\vec{r} = x\hat{i} + y\hat{j}$, $\vec{\tilde{r}} = \tilde{x}\hat{i} + \tilde{y}\hat{j}$, $\vec{r}' = x'\hat{i} + y'\hat{j}$. For simplification it was supposed that the object is illuminated by a plane wave [$E(x, y) = \text{constant}$]. $T_L(k(\vec{r}/\tilde{z} + \vec{r}'/z'))$ is the Fourier transform of the magnitude of the lens transmission function $|A_L(\vec{r})|$,

$$T_L\left(k\left(\frac{\vec{r}}{\tilde{z}} + \frac{\vec{r}'}{z'}\right)\right) = \int |A_L(\vec{r})| \exp\left\{ik\left[\left(\frac{\vec{r}}{\tilde{z}} + \frac{\vec{r}'}{z'}\right) \cdot \vec{r}\right]\right\} d\vec{r}. \quad (5)$$

III. QUANTUM CALCULATION OF THE IMAGE SPATIAL CORRELATION FUNCTION

Figure 1(a) shows a general scheme for obtaining an image with a two-photon light source. Two-photon wave pack-

ets idler and signal are generated by collinear SPDC type I or type II when a nonlinear crystal is illuminated by a pump laser beam. In type I phase matching condition, the idler and signal photons have parallel polarizations and in type II, they have orthogonal ones. The generated photon pairs illuminate an object, and the transmitted idler and signal photons are directed to a lens that generates the image of the object at the image plane. The image is obtained by detecting the photon pairs in coincidence with the detectors signal and idler free to displace transversely at the image plane. The photon pairs are split by a nonpolarizing (type I case) or polarizing (type II) beam splitter. The lens is separated from the object by a distance \tilde{z} and from the image by a distance z' . Those distances are related by the thin-lens equation in accordance with expression (1) where the lens focal length is f .

Calculations were done by using a quantum multimode formalism developed by Mandel and collaborators [5,14]. The number of detected coincident photons is proportional to the spatial quantum fourth-order correlation function $C(\vec{r}_s, \vec{r}_i)$, calculated at the detectors' transverse positions \vec{r}_i and \vec{r}_s ,

$$C(\vec{r}_s, \vec{r}_i) = \langle \Psi | \hat{E}_i^{(-)}(\vec{r}_i) \hat{E}_s^{(-)}(\vec{r}_s) \hat{E}_i^{(+)}(\vec{r}_i) \hat{E}_s^{(+)}(\vec{r}_s) | \Psi \rangle, \quad (6)$$

where $\hat{E}^{(+)}$ and $\hat{E}^{(-)}$ are the positive and the negative parts of the electric field operator. The light state $|\Psi\rangle$ generated by SPDC in the paraxial, monochromatic $[\Delta \omega_j$ (frequency bandwidth) $\ll \omega_j$ (frequency), $j = s, i, p$], and thin crystal approximation is given by [15]

$$|\Psi(t)\rangle = |\text{vac}\rangle + \text{const} \times \int d\vec{q}_s \int d\vec{q}_i \nu(\vec{q}_s + \vec{q}_i) |1, \vec{q}_s\rangle |1, \vec{q}_i\rangle, \quad (7)$$

where $|\text{vac}\rangle$, $|1, \vec{q}_s\rangle$, and $|1, \vec{q}_i\rangle$ are the vacuum, signal, and idler Fock states in the transverse momentum representation, and \vec{q}_s, \vec{q}_i are the signal and the idler transverse momentum. $\nu(\vec{q}_s + \vec{q}_i)$ is the angular spectrum of pump field at the crystal position ($z=0$) and is equal to the Fourier transform of the transverse pump electric field distribution.

In Eq. (6), all information about the object and the lenses are contained in the signal and idler electric field operators. The electric field operators are built by making the electric field operator propagate from the crystal to the object, from the object to the lens and then to the detector. By using paraxial approximation, the resultant electric field operator at the detector position is

$$\begin{aligned} \hat{E}_j^{(+)}(\vec{r}_j, z) = & \text{const} \int d\vec{q}_j \int d\vec{q}'_j \int d\vec{q}''_j a(\vec{q}''_j) \\ & \times T_{aj}(\vec{q}'_j - \vec{q}''_j) T_{lj}(\vec{q}_j - \vec{q}'_j) \\ & \times \exp \left[i \left(\vec{q}_j \cdot \vec{r}_j - \frac{q_j^2}{2k_j} z_j' - \frac{q_j'^2}{2k_j} \tilde{z}_j - \frac{q_j''^2}{2k_j} z_a \right) \right], \end{aligned} \quad (8)$$

where $j = s, i$; z_a is the object-crystal distance, $a(\vec{q}''_j)$ is the destruction operator at the crystal position, and $T_{aj}(\vec{q}'_j - \vec{q}''_j)$, $T_{lj}(\vec{q}_j - \vec{q}'_j)$ are the Fourier transforms of the object $A_j(\vec{r})$ and lens $A_{lj}(\vec{r})$ transmission functions, respectively. By substituting the signal and idler electric field operators (8) in Eq. (6), we notice that the fourth-order correlation function can be rewritten as

$$C = |g(\vec{r}_s, \vec{r}_i)|^2, \quad (9)$$

where $g(\vec{r}_s, \vec{r}_i)$ is the probability amplitude for detecting the signal and idler photons at the image plane at transverse positions \vec{r}_s and \vec{r}_i , respectively,

$$\begin{aligned} g(\vec{r}_s, \vec{r}_i) = & \text{const} \int d\vec{q}_i \int d\vec{q}_s \int d\vec{q}'_i \int d\vec{q}'_s \int d\vec{q}''_i \\ & \times \int d\vec{q}''_s \nu(\vec{q}''_s + \vec{q}''_i) T_{as}(\vec{q}'_s - \vec{q}''_s) T_{ls}(\vec{q}_s - \vec{q}'_s) \\ & \times T_{ai}(\vec{q}'_i - \vec{q}''_i) T_{li}(\vec{q}_i - \vec{q}'_i) \\ & \times \exp \left[i \left(\vec{q}_s \cdot \vec{r}_s - \frac{q_s^2}{2k_s} z_s' - \frac{q_s'^2}{2k_s} \tilde{z}_s - \frac{q_s''^2}{2k_s} z_{as} \right) \right] \\ & \times \exp \left[i \left(\vec{q}_i \cdot \vec{r}_i - \frac{q_i^2}{2k_i} z_i' - \frac{q_i'^2}{2k_i} \tilde{z}_i - \frac{q_i''^2}{2k_i} z_{ai} \right) \right]. \end{aligned} \quad (10)$$

For the collinear two-photon generation, $z_{as} = z_{ai}$. By writing explicitly the Fourier transforms of the object and lens transmission functions, and the angular spectrum of the pump field (the Fourier transform of the pump transverse electric field distribution) in Eq. (10), we can rewrite the probability amplitude $g(\vec{r}_s, \vec{r}_i)$ as

$$\begin{aligned} g(\vec{r}_s, \vec{r}_i) = & \text{const} \int d\vec{\alpha} \int d\vec{\beta} \int d\vec{\xi} \int d\vec{\eta} A_{ls}(\vec{\alpha}) A_{li}(\vec{\beta}) \\ & \times A_{ai}(\vec{\xi}) A_{as}(\vec{\eta}) W \left(\frac{\vec{\eta}}{\mu_i} + \frac{\vec{\xi}}{\mu_s}, z_a \right) \\ & \times \exp \left[\frac{ik_p |\vec{\xi} - \vec{\eta}|^2}{2\mu_s \mu_i z_a} \right] \exp \left[\frac{ik_s |\vec{r}_s - \vec{\alpha}|^2}{2z_s'} \right] \\ & \times \exp \left[\frac{ik_i |\vec{r}_i - \vec{\beta}|^2}{2z_i'} \right] \exp \left[\frac{ik_s |\vec{\alpha} - \vec{\xi}|^2}{2\tilde{z}_s} \right] \\ & \times \exp \left[\frac{ik_i |\vec{\beta} - \vec{\eta}|^2}{2\tilde{z}_i} \right], \end{aligned} \quad (11)$$

where $\alpha, \beta (\xi, \eta)$ are the transverse spatial coordinates at the lens (object) plane and $W(\vec{\rho}, z_a)$ is the transverse pump electric field distribution at position z_a . We also define the quantities: z_a by the relation $k_p/z_a = k_s/z_{as} + k_i/z_{ai}$ and μ_j as $\mu_j = (k_p/z_a)(z_{aj}/k_j)$ with $j = i, s$.

Expression (11) can be further simplified because so far it is valid for any object and lens transmission functions, for

any transverse pump profile, and for any detector scan procedure. It is also independent of the two-photon generation type, being the same for collinear or noncollinear geometry. Our goal is to obtain an expression for $g(\vec{r}_s, \vec{r}_i)$ that resembles the coherent classical transverse electric field (4) at the image plane so that we can compare the classical and quantum results. We start by substituting in Eq. (11) the lens transmission functions $A_j(\vec{\gamma})$ ($j=i, s, \gamma=\alpha, \beta$), defined in Eq. (3). Then, we use the thin-lens equation (1) in Eq. (11), and obtain

$$g(\vec{r}_s, \vec{r}_i) = \text{const} \times \int d\vec{\alpha} \int d\vec{\beta} \int d\vec{\xi} \int d\vec{\eta} |A_{ls}(\vec{\alpha})| |A_{li}(\vec{\beta})| \\ \times A_{ai}(\vec{\xi}) A_{as}(\vec{\eta}) W\left(\frac{\vec{\eta}}{\mu_i} + \frac{\vec{\xi}}{\mu_s}, z_a\right) \exp\left[-i\left(\frac{k_s}{z_s} \vec{r}_s + \frac{k_s}{z_s} \vec{\xi} \cdot \vec{\alpha}\right)\right] \exp\left[-i\left(\frac{k_i}{z_i} \vec{r}_i + \frac{k_i}{z_i} \vec{\eta} \cdot \vec{\beta}\right)\right], \quad (12)$$

where we have neglected the quadratic exponentials in the variables $\vec{\xi}$ and $\vec{\eta}$ by assuming that the objects are small as compared with the longitudinal distances involved. The exponentials

$$\exp\left[\frac{ik_s}{2z_s} \vec{r}_s^2\right] \exp\left[\frac{ik_i}{2z_i} \vec{r}_i^2\right]$$

were also omitted for not contributing to the coincidence rate (9). The above probability amplitude can be rewritten as

$$g(\vec{r}_s, \vec{r}_i) = \text{const} \times \int d\vec{\xi} \int d\vec{\eta} A_{ai}(\vec{\xi}) A_{as}(\vec{\eta}) W\left(\frac{\vec{\eta}}{\mu_i} + \frac{\vec{\xi}}{\mu_s}, z_a\right) \\ \times T_{ls}\left[k_s\left(\frac{\vec{r}_s}{z_s} + \frac{\vec{\xi}}{z_s}\right)\right] T_{li}\left[k_i\left(\frac{\vec{r}_i}{z_i} + \frac{\vec{\eta}}{z_i}\right)\right], \quad (13)$$

where T_{lj} is the Fourier transform of the magnitude of the lens transmission functions $|A_j(\vec{\gamma})|$ ($j=i, s, \gamma=\alpha, \beta$). By comparing the two-photon probability amplitude (13) with the classical electric field (4) at the image plane, we notice that the classical and quantum results are different. The pump transverse electric field distribution at z_a prevents Eq. (13) from being rewritten as a product of the idler and signal independent expressions, as it would be in an analogous classical configuration.

Expression (12) or (13) is still not analogous to the classical image expression (4), and some modifications are needed. We propose three experimental schemes for obtaining an image from the object when photon pairs are used. Figure 2(a) shows the first proposed experimental setup, which we call setup 1. In this configuration, $z_{as} = z_{ai} = z_a$, where z_a is the crystal-object distance. Three modifications were done to setup 1 for simplifying expression (12). First, the idler and signal photons are not generated collinearly and

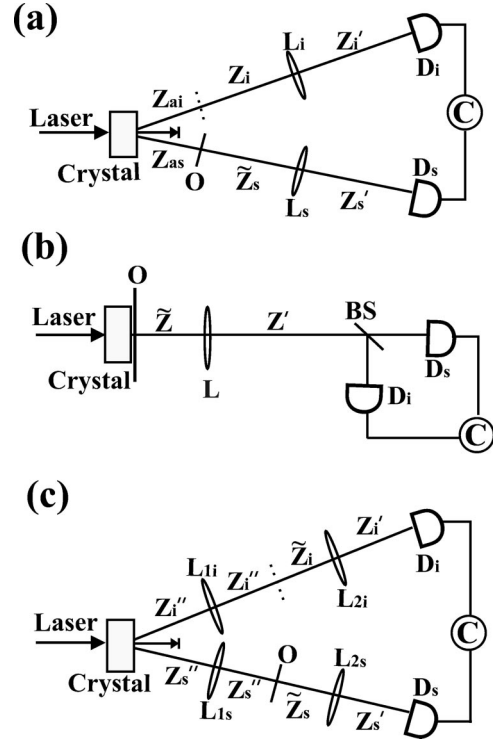


FIG. 2. (a) Outline of the optical setup for observing the image of an object illuminated by noncollinear parametric down-converted photon pairs, after a laser beam is incident in type II crystal. The image is detected in coincidence at the image plane by signal D_s and idler D_i detectors, after the idler photon is transmitted through the object (O). L_j is a lens, z_{aj} is the crystal-object distance, \tilde{z}_j is the object-lens distance, and z' is the lens-image distance, for idler (i) and signal (s) photons with $j=i, s$. Dotted line means that there is no object at the signal path. (b) Optical setup similar to Fig. 1(a), except that the object (O) is placed close to the crystal $z_a \approx 0$. (c) Optical setup similar to Fig. 2(a), except that lenses L_{1j} are used for forming a two-photon image of the crystal at the object position. L_{2j} are used for forming a two-photon image of the object at the detector position. z'' is the crystal- L_{1j} distance, z''' is the L_{1j} -object distance, \tilde{z}_j is the object- L_{2j} distance, and z' is the L_{2j} -image distance.

only the idler photon will pass through the object, which implies that $A_{as}(\vec{\eta}) = 1$. The second modification is that the pump beam is focused at the object position z_a so that $W(\vec{\eta}/\mu_i + \vec{\xi}/\mu_s, z_a)$ can be approximated by a δ function $\delta(\vec{\eta}/\mu_i + \vec{\xi}/\mu_s)$. The third implementation is that the signal and idler photons are detected such that $\vec{r}_s = -\vec{r}_i \equiv \vec{r}$, which means that the idler and signal detectors are scanned simultaneously in opposite directions (see Ref. [16] for a similar detection scheme). In Fig. 2(a), we considered that the lens-object and the lens-detector distances are the same, and therefore, $z'_s = z'_i \equiv z'$, $\tilde{z}_s = \tilde{z}_i \equiv \tilde{z}$. A further simplification is to consider that the idler and the signal have the same wavelength, such that $k_s = k_i = k_p/2$ and $\mu_i = \mu_s = 2$. The modified expression for $g(\vec{r}_s, \vec{r}_i)$ is

$$g(\vec{r}, -\vec{r}) = \text{const} \times \int d\vec{\xi} A_{ai}(\vec{\xi}) \int d\vec{\alpha} \int d\vec{\beta} |A_{ls}(\vec{\alpha})| |A_{li}(\vec{\beta})| \times \exp \left[-ik_p \left(+\frac{\vec{r}}{z'} + \frac{\vec{\xi}}{z} \right) \cdot \left(\frac{\vec{\alpha} - \vec{\beta}}{2} \right) \right]. \quad (14)$$

This last expression for $g(\vec{r}_s, \vec{r}_i)$ is still not analogous to the classical electric field at the image plane (4). We define the new variables \vec{u} and \vec{v}

$$\frac{\vec{\alpha} + \vec{\beta}}{2} = \vec{u}, \quad \frac{\vec{\alpha} - \vec{\beta}}{2} = \vec{v}, \quad (15)$$

and rewrite Eq. (14) as

$$g(\vec{r}, -\vec{r}) = \text{const} \times \int d\vec{\xi} A_{ai}(\vec{\xi}) T_F \left[k_p \left(\frac{\vec{r}}{z'} + \frac{\vec{\xi}}{z} \right) \right]. \quad (16)$$

$T_F[k(\vec{r}/z' + \vec{\xi}/z)]$ is the Fourier transform of the convolution of the lens transmission functions $F(\vec{v})$:

$$T_F \left[k_p \left(\frac{\vec{r}}{z'} + \frac{\vec{\xi}}{z} \right) \right] = \int d\vec{v} F(\vec{v}) \exp \left[-ik_p \left(+\frac{\vec{r}}{z'} + \frac{\vec{\xi}}{z} \right) \cdot \vec{v} \right], \quad (17)$$

which is defined as

$$F(\vec{v}) = \int d\vec{u} |A_{ls}(\vec{u} + \vec{v})| |A_{li}(\vec{u} - \vec{v})| = |A_{ls}(2\vec{v})| * |A_{li}(2\vec{v})|. \quad (18)$$

Now, $g(\vec{r}_s, \vec{r}_i)$ is written in an analogous form to the coherent classical electric field at the image plane (4). By comparing the two expressions, we notice two differences. The image described by $g(\vec{r}_s, \vec{r}_i)$ is affected by the Fourier transform of a nonlocal lens whose transmission function is equal to $F(\vec{v})$. We call this effective lens nonlocal because its transmission function $F(\vec{v})$ is obtained by calculating the convolution of the magnitude of the idler and signal lens transmission functions. $F(\vec{v})$ cannot be written as a product of independent idler and signal lens transmission functions. Nonlocality appears at the fourth-order correlation function because the photon pairs are in a transverse momentum entangled state (7). This feature cannot be obtained by doing the same experiment with some kind of synchronized emitter of coherent classical light (two synchronized pulsed laser beams, for example). In this last case, the fourth-order correlation function at the image plane would be the product of idler and signal independent transmitted light intensities. The second difference is that the wave vector that appears in Eq. (16) is the wave vector of the pump laser k_p and not the wave vector of the down-converted photons.

For arriving at expression (16) we assumed that the focused laser beam at the object position has a transverse profile width sufficiently narrow to be described by a δ function.

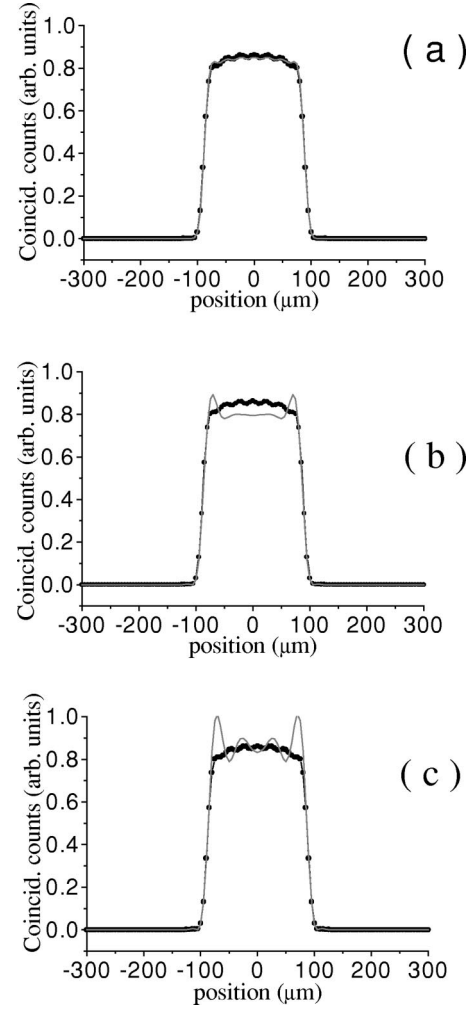


FIG. 3. Calculated coincidence rate at the image plane of a 15- μm width slit as an object, positioned at $x=0$. The gray continuous line plots show the coincidence rate calculated with the $1/e$ full width of the Gaussian laser profile at the object position equal to 1 μm in (a), 3 μm in (b), and 10 μm in (c). Slit length is considered infinite. Square lenses' lengths $2L$ are 3.6 cm. The distance between the crystal and the object is $z_a=40$ cm, between the lens and the image plane is $z'=92.5$ cm, and between the object plane and the lens is $z=7.5$ cm. In (a), (b), and (c) is also plotted the fourth-order correlation function at the image plane for the same slit when the pump laser beam transverse width is described by a δ function (continuous black line with dots).

Sufficiently narrow means that the Gaussian profile width (for example, full width at $1/e$ maximum value) is much smaller than the smallest dimension of the object to be imaged. We have checked this by doing numeric simulation of the coincidence rate at the image plane for different pump laser beam Gaussian profile widths compared with the dimension of a unidimensional object. Figure 3 shows the calculation of the fourth-order correlation function at the image plane [expressions (9) and (13)] for a one-dimensional slit as an object at the idler path with $15\mu\text{m}$ width. For this simulation, we assume $A_{as}(\vec{\eta})=1$; $k_s=k_i=k_p/2$ and $\mu_i=\mu_s=2$ ($\lambda_s=\lambda_i=826$ nm); $r_s=-r_i\equiv r$; a square lens with dimen-

sions $2L$, with $L=1.8$ cm; $z'_s=z'_i=92.5$ cm and $\tilde{z}_s=\tilde{z}_i=7.5$ cm. The $1/e$ full width of the Gaussian transverse laser profile at the object position was chosen to be $1\mu\text{m}$ in Fig. 3(a), $3\mu\text{m}$ in Fig. 3(b), and $10\mu\text{m}$ in Fig. 3(c). In Figs. 3(a)–3(c), the fourth-order correlation function at the image plane for the same slit is also plotted when the pump laser beam transverse profile is described by a δ function (continuous line with dots). It is clear that when the laser profile width is much smaller than the slit's width, the calculated fourth-order correlation function is identical to the one calculated with a δ pump beam transverse profile [Fig. 3(a)]. This approximation may not be always a good approximation. We analyze a second experimental setup where the laser beam is not focused at the object position and this approximation, therefore, is not necessary. We call it setup 2 and is shown in Fig. 2(b). In this setup, the object is placed at the crystal position, just after the crystal such that $z_a \approx 0$.

The probability amplitude for detecting the signal and idler photons at the image plane for this new configuration cannot be calculated by simply making $z_a=0$ in Eq. (10). First, we have to write the electric field operator for the modified configuration shown in setup 2 [Fig. 2(b)]:

$$\begin{aligned} \hat{E}_j^{(+)}(\vec{r}_j, z) = & \text{const} \times \int d\vec{q}_j \int d\vec{q}'_j \int d\vec{q}''_j a(\vec{q}''_j) T_{aj}(\vec{q}'_j - \vec{q}''_j) \\ & \times T_{lj}(\vec{q}_j - \vec{q}'_j) \exp \left[i \left(\vec{q}_j \cdot \vec{r}_j - \frac{q_j^2}{2k_j} z_j - \frac{q_j'^2}{2k_j} \tilde{z}_j \right) \right]. \end{aligned} \quad (19)$$

Except for the absence of an exponential term containing z_a , Eq. (19) is identical to Eq. (8). By following the same procedure used above for calculating the coincidence rate, we arrive at a similar expression for the two-photon amplitude probability at the image plane

$$\begin{aligned} g(\vec{r}_s, \vec{r}_i) = & \text{const} \times \int d\vec{\alpha} \int d\vec{\beta} \int A_{ls}(\vec{\alpha}) A_{li}(\vec{\beta}) \\ & \times W_a \left(\frac{\vec{\alpha}}{\mu_i} + \frac{\vec{\beta}}{\mu_s}, z_l \right) \exp \left[\frac{ik|\vec{\alpha} - \vec{\beta}|^2}{2\mu_s \mu_i z_l} \right] \\ & \times \exp \left[\frac{ik_s(\vec{r}_s - \vec{\alpha})^2}{2z'_s} \right] \exp \left[\frac{ik_i(\vec{r}_i - \vec{\beta})^2}{2z'_i} \right], \end{aligned} \quad (20)$$

where z_l is defined by the relation

$$\frac{k_p}{z_l} = \frac{k_s}{z'_s} + \frac{k_i}{z'_i}. \quad (21)$$

$W_a(\vec{\alpha}/\mu_i + \vec{\beta}/\mu_s, z_l)$ is the transverse profile of the laser beam at position z_l after being transmitted through the object

$$\begin{aligned} W_a \left(\frac{\vec{\alpha}}{\mu_i} + \frac{\vec{\beta}}{\mu_s} \right) = & \int d\vec{\xi} A_{ai}(\vec{\xi}) A_{as}(\vec{\xi}) W(\vec{\xi}, 0) \\ & \times \exp \left[\frac{ik \left| \frac{\vec{\alpha}}{\mu_i} + \frac{\vec{\beta}}{\mu_s} - \vec{\xi} \right|^2}{2z_l} \right]. \end{aligned} \quad (22)$$

We notice that it is the product of the object transmission functions $A_{ai}(\vec{\xi}) A_{as}(\vec{\xi})$ that is present in Eq. (22) and not simply $A_{ai}(\vec{\xi})$. Therefore, in general, the detected image in setup 2 does not reproduce the object. Nevertheless, for the particular case where the object is made up of a number of cells described by a binary function (transmission function has values 0 or 1), $A_{ai}(\vec{\xi}) A_{as}(\vec{\xi}) = A_{ai}(\vec{\xi})$, and we can obtain the image of the object. Besides the restriction for the object being binary, we impose that the detection is done such that $\vec{r}_s = \vec{r}_i \equiv \vec{r}$, which means that both the detectors are scanned in the same direction with the same step when detecting the image. The quadratic exponentials in the variables $\vec{\xi}$ are neglected by assuming that the objects are small as compared to the longitudinal distances involved. We also assume that the transverse pump beam profile is constant at the crystal position, i.e., $W(\vec{\xi}, 0) = \text{const}$. At the image plane where $1/f = 1/z' + 1/z_l$, and for the particular case where the idler and signal photons have the same wavelength ($k_s = k_i = k_p/2$, $\mu_i = \mu_s = 2$), we obtain the following probability amplitude:

$$g(\vec{r}, \vec{r}) = \text{const} \times \int d\vec{\xi} A_{ai}(\vec{\xi}) T_F \left[k_p \left(\frac{\vec{r}}{z'} + \frac{\vec{\xi}}{z} \right) \right], \quad (23)$$

which is equal to expression (16). $T_F[k(\vec{r}/z' + \vec{\xi}/z)]$ is defined as before [see Eq. (17)]. Again, for arriving in Eq. (23), we have defined the new variables \vec{u}, \vec{v} as in Eq. (15).

In setup 2, the object is as close as possible to the crystal and in the ideal case, their separation is zero. This may not be practical because it could be difficult to avoid the UV laser beam incidence on the object during the image measurement. Avoiding the UV light interaction with the object may be useful if the object is sensitive to the UV exposition. We propose an alternative configuration setup 3 [Fig. 2(c)], where the object is far away from the crystal and the laser beam does not reach the object. In setup 3, a lens system is used before the object to form the crystal image at the object plane. Now, the object is placed at the crystal image position (“virtual crystal”) [17]. In this configuration, the idler and signal photons are generated not collinearly such that the object is placed only at the idler beam path, and the image can be obtained for any object, not only for binary ones (see discussion above). The first lens pair is at a distance z''_j from the crystal and z'''_j from the object. The second lens pair is at a distance \tilde{z}_j from the object and z'_j from the detector, with $j=i, s$. In setup 3, we assume that $z''_s, z'''_s, \tilde{z}_s$, and z'_s are equal to the distances $z''_i, z'''_i, \tilde{z}_i$, and z'_i , respectively, and $k_s = k_i = k_p/2$. The probability amplitude for detecting the two photons at the image plane of the object is then

$$\begin{aligned}
 g(\vec{r}_s, \vec{r}_i) = & \text{const} \times \int d\vec{\xi} A_{11i}(\vec{\xi}) \int d\vec{\eta} A_{11s}(\vec{\eta}) \int d\vec{\alpha} \cdot 1 \cdot \int d\vec{\beta} A_{ai}(\vec{\beta}) \int d\vec{\gamma} A_{12s}(\vec{\gamma}) \int d\vec{\tau} A_{12i}(\vec{\tau}) W\left(\frac{\vec{\eta}}{\mu_i}\right. \\
 & \left. + \frac{\vec{\xi}}{\mu_s}, z_i''\right) \exp\left[\frac{ik_p|\vec{\xi} - \vec{\eta}|^2}{2\mu_s\mu_i z_i''}\right] \exp\left[\frac{ik_s|\vec{\alpha} - \vec{\xi}|^2}{2z_s'''}\right] \exp\left[\frac{ik_i|\vec{\beta} - \vec{\eta}|^2}{2z_i'''}\right] \exp\left[\frac{ik_s|\vec{\alpha} - \vec{\gamma}|^2}{2\tilde{z}_s}\right] \\
 & \times \exp\left[\frac{ik_i|\vec{\beta} - \vec{\tau}|^2}{2\tilde{z}_i}\right] \exp\left[\frac{ik_s(\vec{r}_s - \vec{\gamma})^2}{2z_s'}\right] \exp\left[\frac{ik_i(\vec{r}_i - \vec{\tau})^2}{2z_i'}\right], \quad (24)
 \end{aligned}$$

where $W(\vec{\eta}/\mu_i + \vec{\xi}/\mu_s, z_i'')$ is the pump laser transversal profile propagated from the crystal to the first lens pair position,

$$W\left(\frac{\vec{\eta}}{\mu_i} + \frac{\vec{\xi}}{\mu_s}, z_i''\right) = \int d\vec{\rho} W(\vec{\rho}, 0) \exp\left[\frac{ik\left|\frac{\vec{\eta}}{\mu_i} + \frac{\vec{\xi}}{\mu_s} - \vec{\rho}\right|^2}{2z_i''}\right]. \quad (25)$$

In Eq. (24), index 1 refers to the first lens pair that generates the crystal image and index 2 refers to the second lens pair that generates the image of the object. In this work, we are interested in the image formation process of the object and not of the crystal. Therefore, we assume that the lenses $L1$ are infinitely large. An exact copy of the illuminated crystal zone at the object position is formed, with no diffraction and no magnification (we assume $z_j'' = z_j'''$, $j = i, s$). For a small object compared with the longitudinal distances, quadratic exponentials in $\vec{\alpha}$ and $\vec{\beta}$ can be neglected. For a constant profile at the crystal position, the probability amplitude at the image plane is

$$g(\vec{r}, \vec{r}) = \text{const} \times \int d\vec{\xi} A_{ai}(\vec{\xi}) T_F \left[k_p \left(\frac{\vec{r}}{z'} + \frac{\vec{\xi}}{z} \right) \right], \quad (26)$$

where we have imposed that the detection is done in such a way that $\vec{r}_s = \vec{r}_i = \vec{r}$. Equations (16), (23), and (26) are identical, with T_F defined for $L2j$ transmission function magnitudes as in Eq. (17).

IV. DISCUSSION

Equation (16) is the main result of this work. It gives the probability amplitude for detecting photons idler and signal at the image plane for the setups 1–3. Therefore, satisfying the assumptions of each configuration, we arrive at the probability amplitude for detecting the two photons that is analogous to the classical electric field at the image plane. Quantum and classical results can then be compared. The main differences between the two results are the following.

(1) The probability amplitude for detecting the two photons is a function of $\lambda/2(k_p)$, and not of λ (when $k_i = k_s$) as in the classical image formation process. The image is formed as if the object were illuminated by the pump laser beam. This suggests that the image resolution could be better than that obtained when the object is illuminated by a coher-

ent classical light source with the twin photons wavelength.

(2) The quantum image is formed by an effective lens whose transmission function has magnitude $F(\vec{v})$ given by Eq. (18). $F(\vec{v})$ is obtained by doing the convolution between the magnitude of the two lens transmission functions and compressing the resultant function by a factor of 2. The existence of the effective lens demonstrates the nonlocal aspect of the quantum image formation, since the effective lens is nonlocal.

Before we compare the quantum (16) and the classical (4) image predictions, we test the image properties contained in the two-photon probability amplitude $g(\vec{r}_s, \vec{r}_i)$. In all simulations shown below, comparisons were done between the coincidence rate and the classical light intensity at the image plane. For simplicity, the calculation and the plots are done for unidimensional objects. For lenses infinitely large, we expect no diffraction at the formed image. Figures 4(a) and

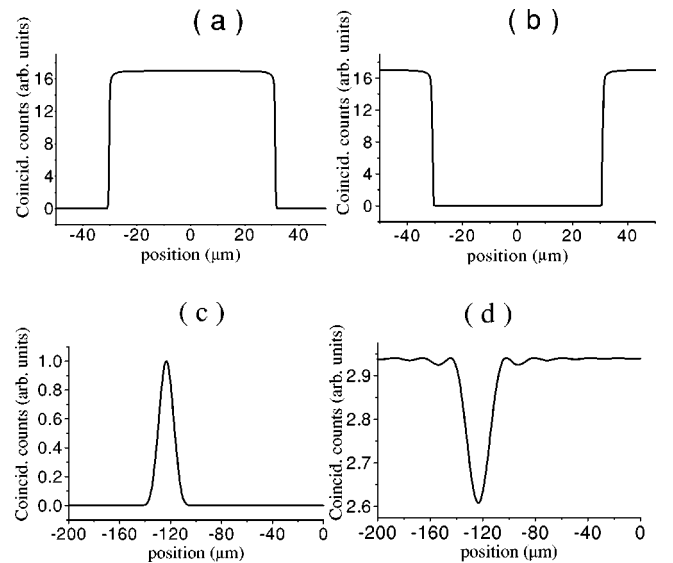


FIG. 4. Calculated coincidence rate at the image plane of a slit (a),(c) and a wire (b),(d) as objects. Objects are positioned at $x = 0$ in (a),(b) and $x = 10 \mu\text{m}$ in (c),(d). The slit width and wire diameter are $5 \mu\text{m}$ in (a),(b) and infinitesimal in (c),(d). Wire and slit lengths are considered infinite. The square lenses' lengths $2L$ are 300 cm in (a),(b) and 3.6 cm in (c),(d). The distance between the crystal and the object is $z_a = 40 \text{ cm}$, between the lens and the image plane is $z' = 92.5 \text{ cm}$, and between the object plane and the lens is $\tilde{z} = 7.5 \text{ cm}$.

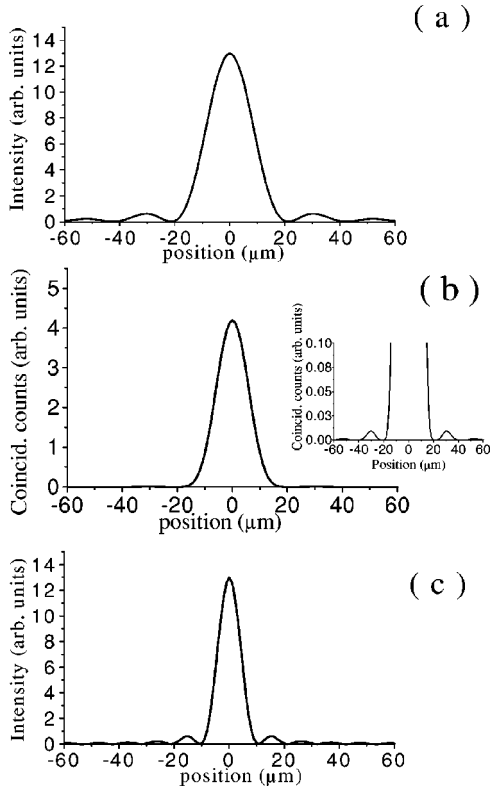


FIG. 5. Light intensity (a),(c) and coincidence rate (b) calculated at the image plane of an infinitesimal slit illuminated by a classical infrared light source (826 nm) in (a); by the idler beam (826 nm) in (b), with idler and signal being detected in coincidence at the image plane; and by a classical light source in the violet (413 nm) in (c). For these calculations, $z' = 92.5$ cm, $\tilde{z} = 7.5$ cm, and $L = 1.8$ cm (inset). The same graph is shown in (b) with amplified scales.

4(b) show the calculated image of a slit and a wire with $5 \mu\text{m}$ width and diameter, respectively. The wire and slit lengths are considered infinite. Calculations were done for two identical square lenses with dimensions $2L$, where L was made 150 cm. The calculation simulates any of the three setups proposed above since they give the same two-photon probability amplitude. For setup 3, the dimensions $2L$ refer to the lenses' index 2. We supposed that the two photons incident at the object have wavelength $\lambda_s = \lambda_i = 826$ nm and are generated by a 413-nm pump laser beam incident in a $\beta\text{-BaB}_2\text{O}_4$ type II parametric down-converter crystal. In all simulations shown below, we have considered $z_a = 40$ cm. The distance between the lens and the image plane is $z' = 92.5$ cm and between the object plane and the lens is $\tilde{z} = 7.5$ cm. As expected, no diffraction is observed in the calculated images shown in Figs. 4(a) and 4(b). Notice in the same figures that the wire diameter and the slit aperture width seen at the image graphs are close to $5 \times 12.3 \mu\text{m}$ due to the image magnification of $m = z'/\tilde{z} = 12.3$. If the lens dimensions are decreased, diffraction effects should appear. This is seen in Figs. 4(c) and 4(d). For this case, the object (slit and wire, respectively) are placed at position $x = 10 \mu\text{m}$ and the image is generated by a lens with dimensions $2L$, with $L = 1.8$ cm. The slit width and wire diameter

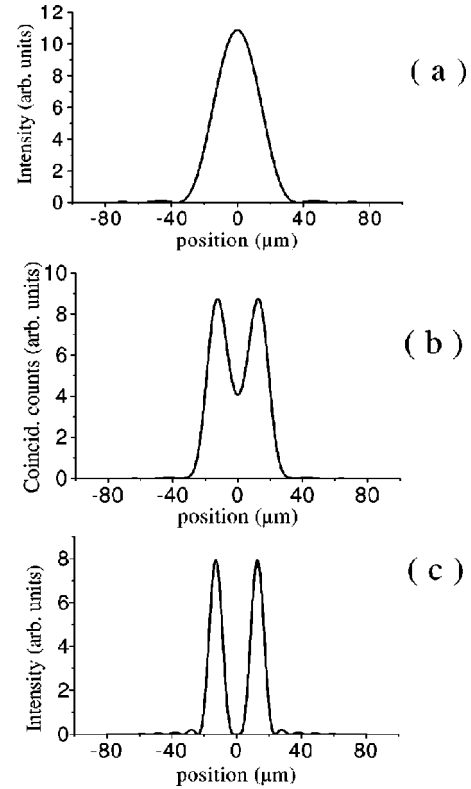


FIG. 6. Light intensity (a),(c) and coincidence rate (b) calculated at the image plane of an infinitesimal double slit illuminated by a classical infrared light source (826 nm) in (a); by the idler beam (826 nm) in (b), with idler and signal being detected in coincidence at the image plane; and by a classical light source in the violet (413 nm) in (c). For these calculations, $z' = 92.5$ cm, $\tilde{z} = 7.5$ cm, and $L = 1.8$ cm. The slits' separation is $2 \mu\text{m}$.

are infinitesimal. All the other parameters, z_a , z' , and \tilde{z} , are the same. We notice that the images are positioned at $x = -123 \mu\text{m}$. Therefore, the magnification is 12.3 and the image is inverted as usual. The next step is to compare the image generated by the twin photons in any configuration shown above (setup 1, for example) with an image generated by a coherent classical light source in a similar setup with wavelength equal to the idler (signal) wavelength ($\lambda_s = \lambda_i = 826$ nm) or equal to the pump wavelength ($\lambda_p = 413$ nm). Therefore, we compare three different image formation process: (1) an object illuminated by a classical light source in the infrared range (826 nm), (2) an object illuminated by the idler beam (826 nm) and the idler and signal photons detected in coincidence at the image plane [see Fig. 2(a)], (3) an object illuminated by a classical light source in the violet (413 nm). These three processes were simulated with the same parameters used above ($z' = 92.5$ cm, $\tilde{z} = 7.5$ cm, and $L = 1.8$ cm). The image of an infinitesimal slit (δ function) illuminated by these three different light sources is shown in Figs. 5(a), 5(b), and 5(c), respectively. By comparing Fig. 5(b) with 5(a) and 5(c), we notice a strong apodization in the quantum image [13]. In the inset of Fig. 5(b), the scale was amplified and this effect is clear. The effective lens has a different transmission function

when compared with the original lens transmission functions, generating a strong reduction of the secondary maxima. On the other hand, at the inset of Fig. 5(b), we notice that the minima are at the same position as those observed in Fig. 5(a), generated by a classical infrared light source. Although the effective wavelength that appears at the quantum image expression is $\lambda_i/2 = \lambda_p$, the effective dimension of the nonlocal lens is half of the original lenses. These two effects compete with each other and the diffraction minima positions in the quantum image [Fig. 5(b)] are not different from their positions in the infrared classical image [Fig. 5(a)]. In Fig. 6, the image of a double slit is calculated again for the three light sources discussed above and for the same parameters used in Fig. 5. We assume that the width of each slit is infinitesimal and their separation is $2 \mu\text{m}$. In these simulations it is shown that the image obtained with the parametric down-converted light source is better resolved than that obtained with the coherent infrared classical light source. In spite of this, the quantum image resolution is not equal to the resolution of the image produced by the violet classical light source. The reason is that the “aperture size” of the effective lens is not equal to the aperture size of the original lenses. This is an important result because it affects the use of down-converted photons in images and lithography applications. We also noticed the presence of a strong apodization in the quantum image, due to the existence of the effective nonlocal lens. This last result points in the direction of the use of correlated photons for obtaining images better resolved than the diffraction limit.

V. CONCLUSION

A quantum multimode formalism was used for calculating the probability amplitude for detecting the parametric down-

converted signal and idler photons at the image plane, after one of them is transmitted through an object. The mathematical expression for the quantum probability amplitude is analogous to the classical electric field at the image plane, which permits the comparison between them. It is shown that the coincidence rate at the image plane gives the image of the object. By comparing with an coherent infrared classical light source with wavelength equal to the parametric down-converted photons λ , we notice two differences. The effective wavelength present at the two-photon probability amplitude is $\lambda/2$. The image is affected by a nonlocal effective lens with a transmission function that is equal to the “compressed” convolution of the idler and signal lens transmission functions. As a result, a strong apodization is observed in the quantum image. It is also shown that the image generated by the parametric down-converted photons is better resolved than a similar one generated by an infrared classical light source, being therefore better than the diffraction limit. In spite of this, the quantum image resolution is not as good as the resolution of the image produced by the pump classical light source because the “aperture size” of the effective lens is not equal to the aperture size of the original lenses. Those results may be useful for real applications with parametric down-converted photons for image generation and quantum lithography.

ACKNOWLEDGMENTS

The authors acknowledge the support of the CAPES, CNPq, PRONEX-SEMICONDUCTORES, and MILÊNIO-INFORMAÇÃO QUÂNTICA. The authors would like to acknowledge Caio Olindo, Oscar Nassif, and Pedro Licínio for very useful discussions.

-
- [1] A. Gatti, E. Brambilla, L.A. Lugiato, and M.I. Kolobov, *Phys. Rev. Lett.* **83**, 1763 (1999).
 - [2] S.K. Choi, M. Vasilyev, and P. Kumar, *Phys. Rev. Lett.* **83**, 1938 (1999).
 - [3] I.V. Sokolov, M.I. Kolobov, and L.A. Lugiato, *Phys. Rev. A* **60**, 2420 (1999).
 - [4] M.I. Kolobov and C. Fabre, *Phys. Rev. Lett.* **85**, 3789 (2000).
 - [5] L. Mandel and E. Wolf, *Optical Coherence and Quantum Optics* (Cambridge University Press, Cambridge, 1995).
 - [6] A.V. Belinskii and D.N. Klyshko, *Zh. Eksp. Teor. Fiz.* **105**, 487 (1994) [*JETP* **78**, 259 (1994)].
 - [7] T.B. Pittman, Y.H. Shih, D.V. Strekalov, and A.V. Sergienko, *Phys. Rev. A* **52**, R3429 (1995); T.B. Pittman, D.V. Strekalov, D.N. Klyshko, M.H. Rubin, A.V. Sergienko, and Y.H. Shih, *ibid.* **53**, 2804 (1996).
 - [8] A.F. Abouraddy, B.E.A. Saleh, A.V. Sergienko, and M.C. Teich, *Phys. Rev. Lett.* **87**, 123602 (2001).
 - [9] A.F. Abouraddy, B.E.A. Saleh, A.V. Sergienko, and M.C. Teich, *J. Opt. Soc. Am. B* **19**, 1174 (2002).
 - [10] J. Jacobson, G. Björk, I. Chuang, and Y. Yamamoto, *Phys. Rev. Lett.* **74**, 4835 (1995).
 - [11] E.J.S. Fonseca, C.H. Monken, and S. Pádua, *Phys. Rev. Lett.* **82**, 2868 (1999).
 - [12] A.N. Boto *et al.*, *Phys. Rev. Lett.* **85**, 2733 (2000); G. Björk, L.L. Sanchez-Soto, and J. Söderholm, *Phys. Rev. Lett.* **86**, 4516 (2001).
 - [13] M.V. Klein and T.E. Furtak, *Optics* (Wiley, New York, 1986).
 - [14] C.K. Hong and L. Mandel, *Phys. Rev. A* **31**, 2409 (1985).
 - [15] C.H. Monken, P.H.S. Ribeiro, and S. Pádua, *Phys. Rev. A* **57**, 3123 (1998).
 - [16] E.J.S. Fonseca, Z. Paulini, P. Nussenzweig, C.H. Monken, and S. Pádua, *Phys. Rev. A* **63**, 043819 (2001).
 - [17] D.N. Klyshko, *Zh. Eksp. Teor. Fiz.* **83**, 1313 (1982) [*JETP* **56**, 753 (1982)].